The Plant Cell, Vol. 20: 2293–2306, September 2008, www.plantcell.org

RESEARCH ARTICLES

A Protracted and Dynamic Maturation Schedule Underlies *Arabidopsis* Leaf Development [W]

Idan Efroni,[1] Eyal Blum,[1] Alexander Goldshmidt, and Yuval Eshed[2]

Department of Plant Sciences, Weizmann Institute of Science, Rehovot 76100, Israel

Leaf development has been monitored chiefly by following anatomical markers. Analysis of transcriptome dynamics during leaf maturation revealed multiple expression patterns that rise or fall with age or that display age-specific peaks. These were used to formulate a digital differentiation index (DDI) based on a set of selected markers with informative expression during leaf ontogeny. The leaf-based DDI reliably predicted the developmental state of leaf samples from diverse sources and was independent of mitotic cell division transcripts or propensity of specific cell types. When calibrated by informative root markers, the same algorithm accurately diagnosed dissected root samples. We used the DDI to characterize plants with reduced activities of multiple *CINCINNATA* (*CIN*)-*TCP* (*TEOSINTE BRANCHED1, CYCLOIDEA, PCF*) growth regulators. These plants had giant curled leaves made up of small cells with abnormal shape, low DDI scores, and low expression of mitosis markers, depicting the primary role of CIN-TCPs as promoters of differentiation. Delayed activity of several CIN-TCPs resulted in abnormally large but flat leaves with regular cells. The application of DDI has therefore portrayed the *CIN-TCPs* as heterochronic regulators that permit the development of a flexible and robust leaf form through an ordered and protracted maturation schedule.

INTRODUCTION

Organogenesis is a sequentially coordinated process that leads to the transformation of a limited number of initial cells into discrete organs with unique shapes and sizes (Conlon and Raff, 1999; Day and Lawrence, 2000). The flat structure of the leaf lamina allows its form to be studied in a simple, nearly two-dimensional context. The continuous process of typical dicot leaf ontogeny and morphogenesis (Avery, 1933) has been divided into phases based on anatomical hallmarks and developmental potentials (Hagemann and Gleissberg, 1996; Poethig, 1997). During the 24- to 48-h-long first stage of primordium initiation, a rod-like, 20- to 40-μm-wide organ is formed and a stable partitioning of the primordium into abaxial and adaxial domains is gradually established (Pekker et al., 2005; Reinhardt et al., 2005). The specification of the adaxial and abaxial domains is followed by initiation of the primary morphogenesis (PM) stage, which is characterized by lateral and distal expansion of a flat lamina. The final stages of leaf morphogenesis are achieved during secondary morphogenesis (SM), when organ expansion and histogenesis are characterized by extensive cell expansion, often associated with multiple endocycles, and limited mitotic divisions (Donnelly et al., 1999). Our understanding of the molecular events that regulate the PM phase, during which the major parts of the leaf, including its broad flat lamina, leaflets (when applicable), and vascular tissues are formed through extensive mitotic divisions, is fragmented. Activities of the homologous factors *CINICNNATA* (*CIN*) of *Antirrhinum majus*, *LANCEOLATE* (*LA*) of tomato (*Solanum lycopersicum*), and *CIN*-related *TCPs* (*CIN-TCP*) of *Arabidopsis thaliana* were implicated in the regulation of leaf development at this stage (Nath et al., 2003; Palatnik et al., 2003; Ori et al., 2007). The understanding of SM regulation is even more fragmented, owing to the difficult distinction between specification of specialized cell types, such as guard cells and trichomes, and more general maturation processes. Significantly, the overall process of leaf ontogeny is fairly long on a biochemical timescale (days to weeks), yet robust and morphologically predictable.

Which regulators promote the leaf differentiation (ontogeny) program and in what sequence they operate to ensure the leaf's unidirectional developmental advance is presently unknown. Genes with such functions are called heterochronic factors. While commonly used to describe the ontogenic process at the whole organism level (Slack and Ruvkun, 1997; Poethig, 2003), this term is also applicable to temporal changes that take place during the development of discrete organs. To identify heterochronic leaf regulators, a coherent definition of leaf differentiation is first required. Chronological changes during leaf morphogenesis have been traditionally monitored using anatomical markers such as trichomes, guard cells, and vascular cells; however, these suffer from limited resolution. In addition, mutants lacking these cell types may be impaired only in cell fate specification, rather than in the progress of leaf maturation. In this work, we provide a quantitative definition of the dynamic leaf differentiation that is based on the analysis of the developing-leaf transcriptome. We identify numerous markers that display an expression gradient or a transient expression peak in sequential phases of leaf maturation and use these markers to develop a

[1] These authors contributed equally to this work.

[2] Address correspondence to yuval.eshed@weizmann.ac.il.

The author responsible for distribution of materials integral to the findings presented in this article in accordance with the policy described in the Instructions for Authors (www.plantcell.org) is: Yuval Eshed (yuval.eshed@weizmann.ac.il).

[W] Online version contains Web-only data.

www.plantcell.org/cgi/doi/10.1105/tpc.107.057521

differentiation score based on transcriptome snapshots. The calculated differentiation score is shown to accurately predict the developmental stage of a diverse set of leaf samples as well as intraleaf differentiation gradients.

The differentiation score was used to further analyze the function of the *CIN*-related *TCPs* (*CIN-TCP*), a class of leaf development regulators active during the PM stage (Palatnik et al., 2003; Ori et al., 2007). Members of the *TCP* family have been implicated in both positive and negative regulation of cell proliferation and have been partitioned on this basis into two classes. Class I members are directly associated with promotion of the cell cycle machinery (Kosugi and Ohashi, 2002; Li et al., 2005), while members of class II, such as *CIN*, were implicated in priming leaf cells for a cell cycle arrest signal (Nath et al., 2003). Five *Arabidopsis CIN-TCPs* are negatively coregulated by *miR319* and have been implicated in shaping leaves (Palatnik et al., 2003). Downregulation of their activities led to extended proliferation of cells along leaf margins, resembling *cin* mutants in *Antirrhinum* (Nath et al., 2003). However, expression analyses of some of these *CIN-TCPs* revealed extensive expression during the proliferative phase of leaf development, suggesting a more complex relationship with the cell division machinery (Palatnik et al., 2003; Koyama et al., 2007; Ori et al., 2007). Using the transcriptome-based differentiation score, we characterized *Arabidopsis* plants with reduced activities of all eight *CIN-TCPs*. Scoring their transcriptome shortly after leaf initiation indicated an overall delay in the accumulation of differentiation transcripts, together with reduced expression of markers for mitotic activity. The early elimination of differentiation programs resulted sequentially in sustained mitotic divisions and a failure to enter the normal cell expansion of the SM phase. Taken together, our analysis shows that *CIN-TCP* genes act as true heterochronic regulators of leaf development. Indeed, by imposing a transient temporal delay, rather than complete abolishment of their activities, large leaves with normal cell morphology at maturity were realized. We propose that during leaf development, transient and sequential expression of heterochronic factors such as the *CIN-TCPs* provides a robust, yet flexible, mechanism that can integrate physiological inputs to generate a wide range of leaf shapes and sizes.

RESULTS

Transcriptome Dynamics of Leaf Ontogeny

To characterize the transcriptional hallmarks of leaf ontogeny, we analyzed RNA expression profiles extracted from progressively older leaves. This data set (Schmid et al., 2005) was obtained from leaf samples of gradually increasing age from Columbia (Col) ecotype plants grown under continuous light. Among the eight samples, more than half of the expressed genes displayed a larger than twofold change. K-mean clustering of the genes with twofold expression change between minimum and maximum values over development identified two major types of patterns. One type showed a gradual expression gradient, either increasing or decreasing in correlation with leaf developmental age (Figure 1A), and the other type showed transient, abrupt expression, which peaked in a specific time window (Figure 1B). Importantly, when the same gene expression data is randomly scrambled 100 times, the patterns identified favor multiple expression peaks (Figure 1C) rather than single peaks or gradual transitions. These random patterns provided a null hypothesis for pattern prevalence and confirmed the statistically significant enrichment for gradients and single peaks. Notably, clusters of multiple expression peaks or expression troughs were rare (see Supplemental Figure 1 online), indicating that developmental stage is generally identified by the specific presence, rather than absence, of groups of genes (Figure 1B). We therefore concluded that leaf ontogeny is a continuously changing process, with many sequentially operating transcriptional hallmarks defining its progression.

Formulation of a Transcriptome-Based Differentiation Index

The finding that a large number of transcripts exhibit a dynamic behavior during shoot development (Figures 1A to 1C) implies that progressive changes in leaf ontogeny can be quantified. To that end, we designed an algorithm which, in principle, compares the expression level of select genes from a leaf sample of unknown age to expression levels of predefined age marker genes, chosen from an independently collected age defined calibration set (Figure 1D). For the calibration set, we initially used tissue collected from four gradually maturing Landsberg *erecta* (L*er*) plants grown under short days (Figures 1E to 1H, Table 1). As very young leaf primordia could not be separated from the apical meristem, we collected instead shoot apices at two ages, 5 and 14 d after stratification (DAS), containing the shoot apical meristem (SAM) and either two to three or five to six youngest leaves, respectively (Figures 1E and 1F). The range of age estimates for each marker gene expression level was averaged to produce a digital differentiation index (DDI; Figure 1D). Our analysis exposed two major types of expression patterns for age-correlated genes: gradients (Figure 1A) and peaks (Figure 1B). As our (Figures 1E to 1H) and most likely, all other calibration sets cover only part of leaf ontogeny, two artificial time points termed leaf birth and death were added to the calibration set, in which the expression values of all genes was set to 0 (Figures 1I and 1J). This manipulation provided anchoring points that are identical for all possible calibration sets and effectively structured a peak pattern for all age marker genes. Following this transformation, age-correlated marker genes were selected based on the following criteria: they should exhibit at least a twofold change between minimum and maximum expression values among the calibration set samples and have no more than a single expression peak (Figure 1D).

When comparing the normalized expression value of a gene from a sample whose DDI is calculated, it can fall on either side of the expression peak of the same gene in the calibration set and thus produce an ambiguous differentiation score (Figures 1I and 1J). To avoid this, the differentiation scores of the examined sample were determined in two iterative steps. First, age estimations are produced only for those genes that produce unambiguous results, that is, the expression value of the gene sampled is close to the peak value (arbitrarily set at 1/2 the difference of

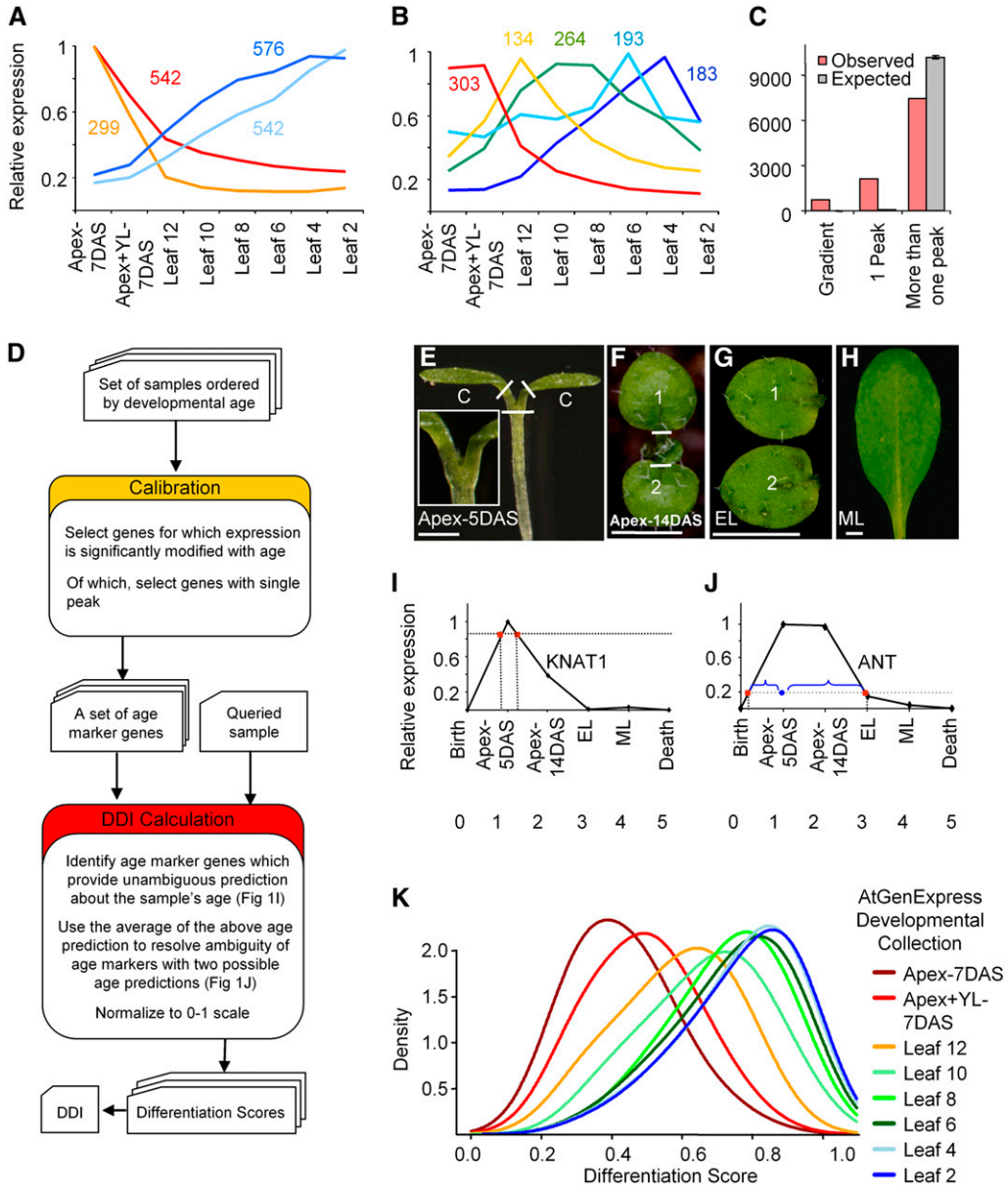

Figure 1. Characterization and Quantification of Leaf Ontogeny Dynamics.

(A) and **(B)** Clusters of genes in which expression is modified across the AtGenExpress leaf developmental stages samples. Leaf 2 is the second leaf formed and, hence, the oldest (see Table 1 for more details). Data were grouped into 25 clusters (each shown in Supplemental Figure 1 online), nine of which are shown here, illustrating either gradual **(A)** or transient **(B)** expression changes during maturation. Numbers indicate cluster size, and lines mark mean normalized expression of all transcripts in the cluster.

(C) Prevalence of the patterns shown in **(A)** and **(B)** compared with 100 randomly permutated data sets (gray bars) and their SD.

(D) Flow chart of the DDI algorithm illustrating the two major steps. Calibration (orange), where a set of age marker genes is isolated, and DDI calculation (red), where, in a two step calculation, differentiation scores are determined for an independent sample.

(E) to **(H)** Samples of gradually maturing L*er* leaves as described in Table 1. The trancriptomes of these samples were used to calibrate the DDI estimates of the AtGenExpress samples. White lines indicate where the tissue was dissected. Inset in **(E)** shows close-up of the collected tissue. C, cotyledons; 1, 2, first two leaves. Bars = 1 cm.

(I) and **(J)** Calculation of a differentiation score based on an unambiguous **(I)** or ambiguous **(J)** marker. The graph shows the behavior of two age markers across the calibration set in the **(E)** to **(H)** samples. The dotted horizontal line indicates a measured value of the gene in a queried sample. The red dots and vertical dotted lines mark the two age predictions that are either averaged **(I)** or preferred by proximity (blue brackets) to the average of all unambiguous differentiation scores (blue dot; **[J]**).

(K) Kernel density plots describing the distribution of differentiation scores extracted for the eight AtGenExpress samples of increasing age. The DDI (average of all differentiation scores) and further description of each sample are listed in Table 1.

Table 1. Samples for Transcriptome Analyses Used in the Course of This Study

	Genotype[a]	Tissue Sampled[b]	Age (DAS)	DDI (This Study) ± SE	DDI (AtGenExpress) ± SE	DDI (Combined) ± SE	DMI ± SE
Data Source: AtGenExpress (Schmid et al, 2005)[c]							
Apex-7DAS	Wild type (Col)	Apex	7	0.429 ± 0.003[1]	0.200 ± 0.000	0.273 ± 0.000	1.194 ± 0.055
Apex+YL-7DAS	Wild type (Col)	Apex + Leaves	7	0.490 ± 0.003[2]	0.299 ± 0.000	0.363 ± 0.000	1.057 ± 0.056
Leaf 12	Wild type (Col)	Leaf 12	17	0.586 ± 0.003[3]	0.400 ± 0.000	0.475 ± 0.002	0.456 ± 0.025
Leaf 10	Wild type (Col)	Leaf 10	17	0.668 ± 0.003[4]	0.500 ± 0.000	0.544 ± 0.001	0.283 ± 0.020
Leaf 8	Wild type (Col)	Leaf 8	17	0.731 ± 0.003[5]	0.599 ± 0.000	0.633 ± 0.001	0.236 ± 0.025
Leaf 6	Wild type (Col)	Leaf 6	17	0.747 ± 0.003[6]	0.698 ± 0.000	0.722 ± 0.001	0.206 ± 0.022
Leaf 4	Wild type (Col)	Leaf 4	17	0.767 ± 0.003[7]	0.800 ± 0.000	0.817 ± 0.001	0.168 ± 0.026
Leaf 2	Wild type (Col)	Leaf 2	17	0.772 ± 0.003[7]	0.898 ± 0.000	0.905 ± 0.001	0.134 ± 0.021
Data Source: This Study[d]							
Apex-5DAS[c]	Wild type (*Ler*)	Apex + Leaves 1–3	5	0.333 ± 0.000	0.381 ± 0.003[2]	0.182 ± 0.000	0.639 ± 0.023
Apex-14DAS	Wild type (*Ler*)	Apex + Leaves 3–7	14	0.499 ± 0.000	0.315 ± 0.002[1]	0.315 ± 0.003	0.982 ± 0.010
EL	Wild type (*Ler*)	Leaves 1 and 2	14	0.665 ± 0.000	0.421 ± 0.003[3]	0.451 ± 0.001	0.463 ± 0.014
ML	Wild type (*Ler*)	Mature leaves 5 and 6	35	0.832 ± 0.000	0.627 ± 0.005[4]	0.592 ± 0.006	0.122 ± 0.013
APEX-14DAS	*glabrous1* (*Ler*)	Apex + Leaves 3–7	14	0.528 ± 0.002	0.322 ± 0.003	0.338 ± 0.003	1.152 ± 0.031
gl1-1 Ler							
Data Source: AtGenExpress (Schmid et al, 2005)[c]							
Petiole	Wild type (Col)	Leaf 7, petiole	17	0.586 ± 0.004[1]	0.510 ± 0.003[1]	0.560 ± 0.004[1]	0.369 ± 0.035
Proximal	Wild type (Col)	Leaf 7, proximal	17	0.743 ± 0.003[2]	0.638 ± 0.002[2]	0.671 ± 0.003[2]	0.204 ± 0.025
Distal	Wild type (Col)	Leaf 7, distal	17	0.765 ± 0.003[3]	0.713 ± 0.002[3]	0.746 ± 0.003[3]	0.139 ± 0.015
Data Source: Schwab et al. (2005)[d]							
	Wild type (Col)	Leaf	~28	0.757 ± 0.003	0.692 ± 0.004	0.638 ± 0.006	0.177 ± 0.035
	35S:miR319a (Col)	Leaf	~28	0.742 ± 0.003	0.625 ± 0.004	0.608 ± 0.006	0.171 ± 0.025
Data Source: This Study[d]							
Apex-14DAS Col	Wild type (Col)	Apex + Leaves 3–7	14	0.471 ± 0.002	0.313 ± 0.003	0.315 ± 0.003[2]	1.004 ± 0.052
-3	*35S:miR-3TCP* (Col)	Apex + Leaves 3–7	14	0.481 ± 0.002	0.299 ± 0.002	0.316 ± 0.003[2]	1.010 ± 0.046
-5	*35S:miR319b* (Col)	Apex + Leaves 3–7	17	0.434 ± 0.003	0.289 ± 0.002	0.262 ± 0.003[1]	0.600 ± 0.027
-8	*35S:miR-3TCP 35S:miR319b* (Col)	Apex + Leaves 3–7	18	0.442 ± 0.003	0.292 ± 0.003	0.263 ± 0.003[1]	0.637 ± 0.038
	pBLS>>rTCP4 (*Ler*)	Apex + Leaves 3–7	14	0.533 ± 0.002	0.361 ± 0.003	0.354 ± 0.003	0.884 ± 0.020

Numbers 1 to 7 indicate statistical significance according to Tukey-Kramer HSD test at $P \leq 0.01$. Different numbers indicate that samples differ significantly. YL, young leaves 1 and 2 that were maintained with the Apex; EL, expanding leaves; ML, mature leaves; -3, reduced 3 *CIN-TCPs*; -5, reduced 5 *CIN-TCPs*; -8, reduced 8 *CIN-TCPs.*

[a] Ecotype background is in parentheses.

[b] To maintain consistency with AtGeneExpress, leaves are numbered according to order of their initiation. Thus, leaf #1 is the first formed and oldest.

[c] Experiments done in triplicates.

[d] Experiments done in duplicates.

adjacent samples; Figure 1I). The average for all of these unambiguous estimations produces a first-round age estimation. In the next step, the rest of the marker genes, which have yielded ambiguous differentiation scores, are incorporated by selecting from the two age possibilities the age that is closet to the first-round age estimation (Figure 1J). Subsequently, the differentiation score provided by each marker is normalized so that 0.0 is birth and 1.0 is death. The average of all differentiation scores of a given sample is the DDI.

To test the DDI algorithm in a simulation study, the relative developmental age of the progressively older Col samples grown in long days (Schmid et al., 2005) was determined by the short-day-grown L*er* calibration set. The distribution prevalence of dynamic expression patterns in this calibration set was similar to that uncovered in the Col set (see Supplemental Figure 2 online), and 3678 age markers met the criteria of showing twofold expression change with age and containing a single expression peak. Differentiation scores for those genes were then calculated for each of the Col ecotype leaf development series samples (Figures 1A and 1B; described in Schmid et al., 2005). A kernel density function was applied for visualization of the score distribution. The differentiation scores of all the samples displayed Gaussian distributions that peaked according to the incremental increase in age (Figure 1K, Table 1). The mean values of those distributions, the DDIs, show a progressive and statistically significant increase in DDI, except for the mild difference between the two oldest leaves (Table 1).

Optimization of the DDI Algorithm through Selection of a Wide-Range Ecotype-Independent Calibration Set

To examine the robustness of the DDI algorithm, it was used to analyze four samples that allow comparisons between two different leaf ages (14-DAS apices and Leaf 12 of Col

background), between leaves of the same age from two different ecotypes (14-DAS apices of Col and L*er* backgrounds), and between leaves of the same age from the wild type and the *glabrous1* trichomeless mutant (14-DAS apices of the L*er* and *gl1* genotypes; see Table 1 for details of all samples). Differentiation scores for the four samples were calculated on the basis of the calibration set described in Figures 1E to 1H (calibration set L*er*). As can be seen in Figure 2A, same-age samples had similar differentiation score distributions, but the mean scores were significantly lower than that of the older Leaf 12 sample. Notably, the distribution of differentiation scores of the 14DAS-L*er* sample, marked as the red line in Figure 2A, left panel, was much narrower than that of all others. This difference stems from the dual use of the sample, as a part of the calibration set and as a queried sample. Indeed, when the eight AtGenExpress samples, which include the Col Leaf 12 sample, were used instead as a calibration set, differentiation score distributions and DDIs of the three same age samples were indistinguishable, while the scores of the Leaf 12 sample had a narrower range (green line, Figure 2A, middle panel). Thus, a larger calibration set provides better resolution power, even when used for samples collected from different ecotypes, different daylengths, and at different labs.

Using the eight AtGenExpress leaf samples as a calibration set, we noted that the DDI ordered the L*er* samples according to age (Table 1); however, the algorithm failed to correctly estimate the age of the youngest sample, Apex-5DAS. This sample is at a less mature developmental stage than all samples in the AtGenExpress collection (Table 1), requiring the algorithm to extrapolate. Taking this observation into consideration, we generated a combined calibration set made up of nine samples with approximately evenly spaced ages selected to include the most extreme ages used in both AtGeneExpress and our studies and comprising a combination of two ecotypes and growth regimes as listed the legend for Figure 2. Using the combined calibration set for the comparison of distribution scores of the same four samples described above resulted in an improved resolution over the Col-only calibration set (cf. Figure 2A middle with right panels; note the elimination of most skewed high scores, larger than ~0.7, for the young Apex samples). The DDI based on the combined calibration set (2164 age markers listed in Supplemental Data Set 1 online) correctly indexed a broader range of ages, showed an increased resolution power, and was adopted as a diagnostic tool for the rest of this study.

While the DDI could capture the relative developmental stage of a measured leaf, the data set used to construct it could be biased by other confounded parameters. For example, the leaf samples from Schmid et al. (2005) differed in age, but also in position, mixing heterophylly with maturation stages. To evaluate the contribution of heterophylly to the calculated DDI, the index was used to characterize the maturation gradient along a single leaf, a gradient previously shown by anatomical and mitotic index considerations (Donnelly et al., 1999). Differentiation scores of samples collected from the same leaf and dissected into petiole, blade proximal, and blade distal portions (Schmid et al., 2005) significantly resolved the known proximo-distal differentiation gradient (Table 1, Figure 2B). Thus, a quantitative expression of an intraleaf maturation gradient was captured, indicating only a minor possible contribution of heterophylly to the DDI used.

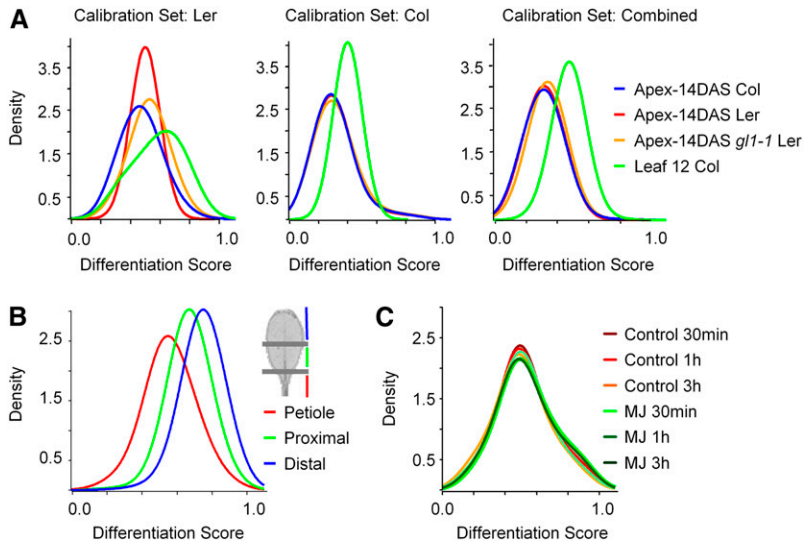

Figure 2. Robustness and Resolution Power of the DDI Algorithm.

(A) to **(C)** Kernel density plots describing the distributions of differentiation scores calculated for samples of various sources by various calibration sets.
(A) Comparison of same-age samples differing in ecotype (L*er* versus Col), same-age samples differing in genotype (*gl1* versus L*er*), or same ecotype samples differing in age (Col Apex versus Leaf 12). Differentiation scores are based on the following calibration sets: the four L*er* samples (Figures 1E to 1H), the eight AtGenExpress Col samples (Schmid et al., 2005), and a combined set based on nine samples selected from both sets to cover a broader developmental range: Apex-5DAS, Apex-7DAS, Apex+YL-7DAS, EL, Leaf 10, Leaf 8, Leaf 6, Leaf 4, and Leaf 2 (see Table 1 for sample details).
(B) A maturation gradient along the plant's 7th leaf captured by a DDI calibrated by the combined set. Inset illustrates the parts of the leaf analyzed.
(C) A uniform DDI of same age plants challenged with methyl jasmonate (Goda et al., 2008), which modified >2000 transcripts among the six treatments.

Mitotic cell divisions, which are most common in young tissues, are also confounded with leaf maturation. To compare the two, a digital mitotic index (DMI) that estimated a transcriptional signature for mitotic activity was formulated. The DMI was defined as the mean normalized expression values of 73 genes previously identified as mitosis marker genes (Menges et al., 2005; Dewitte et al., 2007; listed in Supplemental Data Set 1 online). Examination of DMI scores for the nine gradually maturing leaf samples that make up the DDI calibration set revealed a peak in the Apex-7DAS sample, which is enriched for leaf primordia at the PM stage (see Supplemental Figure 3A online). Indeed, classical observations identified a peak in the dividing cells fraction in leaves at the PM stage relative to either SAMs or initiating leaf primordia (Poethig and Sussex, 1985a; Lyndon, 1998).

While mitotic activity is intimately associated with maturation, it is likely to capture a limited portion of the complex differentiation process. Therefore, different plant organs may share the transcriptional mitotic activity signature while maintaining specific maturation programs. We examined this hypothesis by analyzing DMI and DDI scores of root tissues previously dissected to capture dominant spatiotemporal expression patterns (Brady et al., 2007). While the DMI captured the known peaks of mitotic activity in the root tip and initiating lateral roots, the DDI, which was calibrated by maturing leaf tissues, remained fairly constant (see Supplemental Figure 3B online). However, when the DDI was calibrated with data collected from gradually maturing root samples (Brady et al., 2007), it could capture the developmental progression away from the root tip, but not that of leaf samples (see Supplemental Figures 3C to 3E online). Importantly, the root-calibrated DDI correctly identified the relative age of samples that were first mechanically isolated by distance from the tip and subsequently processed by fluorescence-activated cell sorting to enrich for specific cell types (see Supplemental Figure 3F online; data obtained from Birnbaum et al., 2003). Thus, the algorithm underlying the DDI can operate in an organ-independent manner, can capture developmental state from specific cell types, and is fairly insensitive to the mitotic transcriptional signature per se (see Supplemental Figure 3B online).

Lastly, to examine whether the DDI is sensitive to other unrelated changes in leaf state, the algorithm was applied to the analysis of same age samples challenged by physiological perturbations. In this experiment, six samples of Col seedlings were grown on plates and treated with exogenous jasmonate, and our analysis detected >2000 2× differentially expressed transcripts (data obtained from Goda et al., 2008). However, all of these samples displayed similar distribution of differentiation scores (Figure 2C). Taken together, we can conclude that the DDI can capture the bona fide developmental age of plant organ samples, based solely on their transcriptome. However, as many other factors determine leaf differentiation, growth conditions for the calibration set and queried samples should be properly matched.

Slowly Maturing *cin-tcp* Mutant Leaves Have Low DDI

The DDI algorithm is based on and reflects the ever-changing composition of the leaf. It was next employed to clarify the function of the *CIN*-related *TCPs* (*CIN-TCP*) in the regulation of the temporal progression of leaf development. *CIN-TCPs* make up a class of developmental regulators active transiently during the PM stage (Palatnik et al., 2003; Ori et al., 2007). The *Arabidopsis CIN-TCPs* are phylogenetically divided into two clades. The first includes five members that are coregulated by *miR319*, and the other comprises three *TCP5-like* genes (*TCP5*, *TCP13*, and *TCP17*), which are miR319 insensitive and whose roles in leaf development have not been described to date. Downregulation of the five *miR319*-sensitive TCP genes by overexpression of *miR319* resulted in crinkly leaves (Figure 3C; Palatnik et al., 2003). The loss of *CIN*, the founder *CIN-TCP*, resulted in prolonged cell divisions in *Antirrhinum* leaves (Nath et al., 2003). Similarly, a loss of negative regulation of the tomato *LA* (a *CIN-TCP* homolog) by *miR319* stimulated precocious differentiation (Ori et al., 2007), suggesting that the *CIN-TCPs* might play a role in regulation of developmental timing.

To clarify the role of all *CIN-TCPs* in leaf maturation, particularly in the PM phase, we reduced the activities of all eight by sequential genetic manipulations of the two clades. T-DNA insertion alleles of *tcp5*, *tcp13*, and *tcp17* were obtained from publicly available collections, and homozygous lines had no obvious mutant phenotype. Triple mutants for *TCP5*, *13*, and *17* were then obtained either by conventional breeding or by ubiquitous expression of a corresponding synthetic miRNA (see Supplemental Figure 4 online for miRNA design and comparison with the conventional T-DNA mutants). Downregulation of the other five members (TCP2, 3, 4, 10, and 24) was obtained via overexpression of *miR319a*. Downregulation of *TCP5*, *13*, and *17* in *35S:miR-3TCP* plants stimulated larger leaves and proximal expansion of the blade into the petiole domain (cf. Figures 3A with 3B). Reduction in the activities of the other five *CIN-TCP* genes by overexpressing *miR319* resulted in plants with slow-growing, large, crinkly leaves as described previously (Palatnik et al., 2003; Figure 3C). Dramatic synergic effects on leaf growth were displayed in plants overexpressing both types of miRNAs (referred to as octuple *cin-tcp* for the sake of simplicity). Leaves were dark green, deeply lobed, and highly serrated, exceeding in size both of the parental lines and five times larger than their wild-type counterparts (Figures 3D and 3E; see Supplemental Figure 5 online). Notably, the sequence divergence between the members of the two clades precluded unintended regulation by the endogenous or artificial miRNAs, which in both cases stimulated a specific reduction in the levels of their target transcripts (Figure 3F). The strikingly large size of the octuple *cin-tcp* leaves was associated with slow maturation, evidenced by an ongoing leaf growth and delayed flowering. However, the number of leaves produced before flowering was not significantly altered, indicating that the rate of leaf initiation was greatly reduced relative to wild-type progenitors. Taken together, these results demonstrate that CIN-TCP activities play an additive role in leaf development and are required for programmed arrest of blade growth.

Expression profiles of mature *35S:miR319a* leaves were previously used to determine the target range of the manipulated microRNA (Schwab et al., 2005). The same data set was used here to calculate differentiation scores of these leaves and their corresponding wild type. The DDI of the *35S:miR319a* leaves (0.608 ± 0.006; Table 1) was slightly but significantly lower than

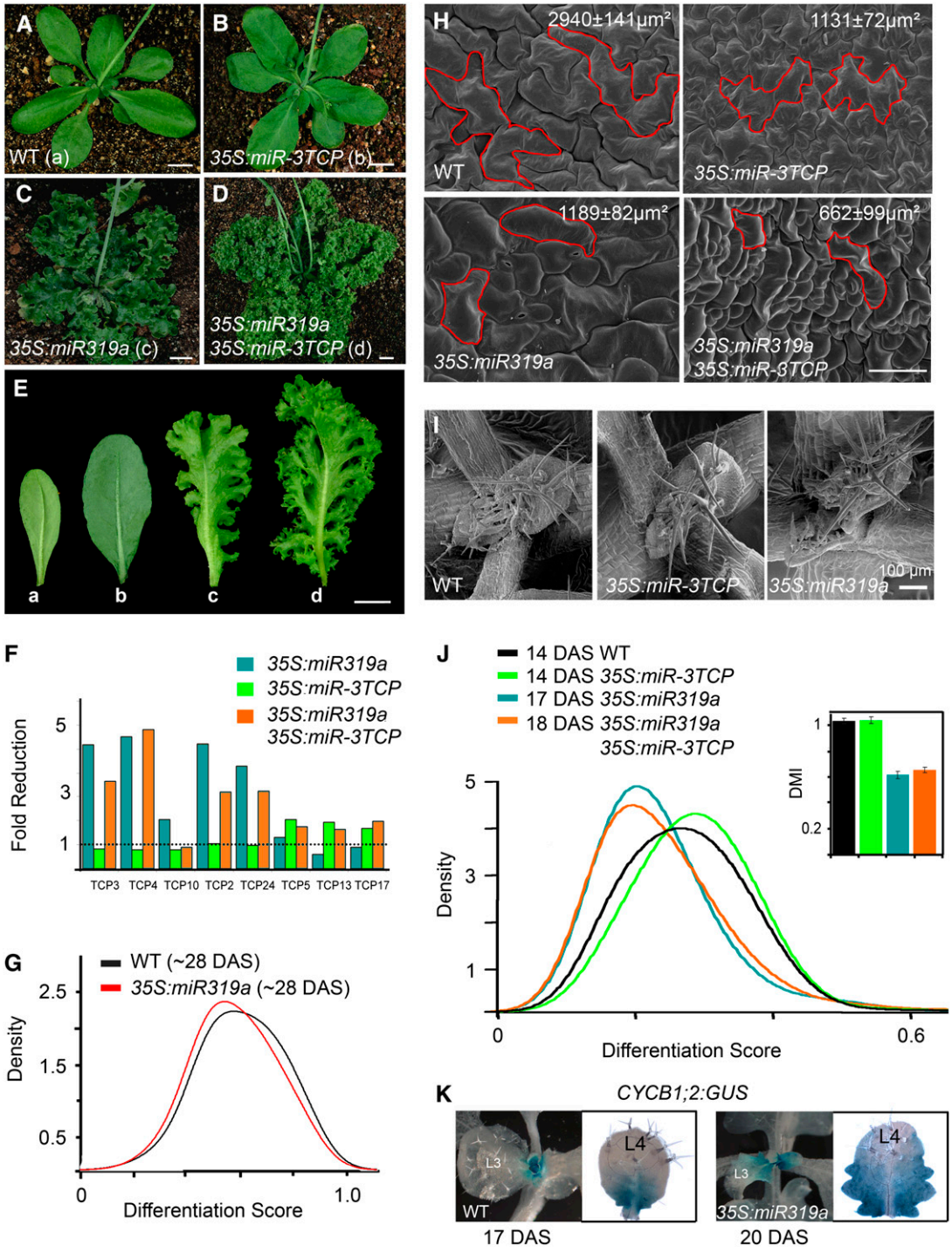

Figure 3. Reduced Activities of *CIN-TCPs* Stimulate Prolonged Growth of Immature Lamina.

(A) to **(D)** Bolting rosettes of plants with gradually reduced *CIN-TCP* levels. Bars = 1 cm.

(E) Fully expanded 6th leaf of the plants in **(A)** to **(D)**.

(F) Fold reduction of specific *TCP* mRNA levels in the different miRNA overexpression lines.

(G) Differentiation score distributions of previously published data of 4-week-old leaf samples (Schwab et al., 2005) capture a mild delayed differentiation in *35S:miR319a*.

(H) Scanning electron micrographs (all shown at the same magnification) of the adaxial epidermal surfaces of the leaves in **(E)**. Note the small size and absence of jigsaw-like cells in *35S:miR319a* blades; cell outlines are marked in red, and average epidermal cell size is at the top left corner. Bars = 50 µM.

normal leaves (0.638 ± 0.006; Table 1), while maintaining similar distribution (Figure 3G), suggesting a role for these TCPs in the regulation of leaf maturation.

Leaf Differentiation, Not Mitotic Cycles, Is a Prime Target of CIN-TCPs

Previous studies on CIN-TCPs in other species have implicated them in the negative regulation of mitotic cell divisions (Nath et al., 2003). We therefore examined cell shape and size in the leaves of the three classes of mutant plants. The mature lamina tissue of the TCP mutant combinations showed a great reduction in cell size (Figure 3H). In addition, cells of *35S:miR319a* leaves lost the typical jigsaw morphology of pavement cells, instead retaining the small, polygonal shape typical of immature cells (Fu et al., 2002). This change of morphology was not apparent in *35S:miR-3TCP* plants (Figure 3H). As expected from the additive effects of the *TCP* genes on leaf size, cells of the giant octuple mutant leaves were ~4.5 times smaller than the wild type, with immature morphology. These observations suggest distinct and additive roles for the three *TCP5*-like and the five *miR319* regulated TCPs.

The reduction in cell size and the immature morphology of mature octuple mutant blade cells could reflect a general heterochronic attribute affecting a wide range of maturation progression characteristics. We wished to examine this using DDI early in leaf development, in tissues that develop shortly after *CIN-TCP* genes are normally activated. To this end, equivalent samples of wild-type and *35S:miR-3TCP* mutant plants were collected at 14 DAS (SAM with five young leaves attached, excluding cotyledons and first two leaves; Figure 3I). As the young leaves of 35S: *miR319a* plants displayed slower expansion relative to those of the wild type and *35S:miR-3TCP*, they were collected 3 to 4 d later. Despite the delayed sampling of mutant leaves expressing *35S: miR319a*, their DDI scores were lower than those of the wild type (Table 1). Moreover, distribution of their differentiation scores was normal and made up simply of an overall shift (Figure 3J).

If the *CIN-TCPs* were primarily mitotic regulators, the shift in maturity could be a secondary effect of extended cell divisions. For example, it has been shown that overexpression of the cell cycle regulator CYCD3;1 results in slowly maturing half-sized leaves with 18 times more cells (Dewitte et al., 2003). In attempt to determine the primary target of the *CIN-TCP*, we measured the transcriptional mitotic signature, the DMI, of wild-type and *cin-tcp* knockdown plants. Despite the dramatic increase in cell number of *35S:miR319a* mature leaves, the calculated DMI of young leaves was almost half that of the wild type (Table 1, Figure 3J). To clarify the apparent disparity, distribution of mitotic cell divisions was monitored by *CYCB1;2:GUS* expression (Donnelly et al., 1999). in the wild type, young leaves of the Apex-14DAS stage, which was used for the transcriptome analysis, displayed uniform staining. In older leaves, staining was gradually limited proximally (Figure 3K). Distal exclusion of marker expression was delayed in *35S:miR319a* leaves, as was shown earlier for the *cin* mutant leaves of *Antirrhinum* (Nath et al., 2003), and the shape of the front arrest was significantly modified (Figure 3K). While mitotic activity is reduced in primordia of *tcp* leaves (Figure 3J), it is subsequently maintained for a longer period of time relative to the wild type (Figure 3K), leading to leaves made of many more cells. The delayed entry into the SM phase of leaf development reflects a slow maturation program in *cin-tcp* leaves. The reduced mutant leaf DDI, together with a significantly low mitotic cell cycle index, thus supports a primary role for *CIN-TCP* in promoting tissue differentiation.

Precocious Activation of the Leaf Maturation Program Yields Miniature Leaves

Genes with heterochronic attributes likely control differentiation in a phase-dependent manner attuned to a window of developmental opportunity. For example, precocious activity of TCP4 in *Arabidopsis* or tomato shoots leads to their precocious arrest (Palatnik et al., 2003; Ori et al., 2007), while normal expression during the proliferative PM stage yields normal leaves. To gain insight into the processes of leaf differentiation influenced by *CIN-TCPs*, we developed an experimental system that would mildly alter *CIN-TCP* temporal expression.

To facilitate such manipulations, the L*er* in silico expression database was used to select promoters of genes displaying a single peak of transient expression at sequential stages of leaf development (see Supplemental Figure 6A online). The transient nature and spatial characteristics of the expression mediated by these promoters was monitored first through transactivation of visual reporters, such as β-glucuronidase (GUS) and green fluorescent protein (GFP) (Figures 4A and 4B). It was then monitored using functional reporters, such as *miR165*, which has been shown to induce SAM abortion or leaf radialization when expressed in the SAM or very young leaves (Alvarez et al., 2006). The selected set of promoters included *pKAN1* (At5g16560), *pGH3.3* (At2g23170), *pBLS* (At3g49950), *p7470* (At2g17470), and *p650* (At1g13650). Of this set, *pKAN1* and *pGH3.3* are active during primordia initiation, with abaxial *pKAN1* activity ceasing early during PM. Activity from *pGH3.3* initiates at plastochron 1 (P1, the first sign of cells bulging from the SAM periphery) and stops at P3 to P4, whereas activity from *pBLS* is initiated and maintained solely in the young lamina, from P3 to P7 (Lifschitz et al., 2006). Lastly, the transient expression of *p7470*

Figure 3. (continued).

(I) Wild-type, *35S:miR-3TCP*, and *35S:miR319a* shoots used for the DDI analysis in **(J)**. The images show the actual material used after removal of all older tissues.

(J) Delayed maturation in *cin-tcp* shoots. The differentiation-score distributions of the samples shown in **(I)**. The *35S:miR319a* samples were 3 to 4 d older but the same size as wild type samples and had a dramatically lower transcription of mitosis genes captured by DMI (inset).

(K) Expression of the mitotic *CYCB1;2:GUS* marker (blue color) in wild-type and *35S:miR319a* plants. Note the prolonged maintenance of mitotic activities in leaf 3 (L3) of plants with reduced CIN-TCP activities.

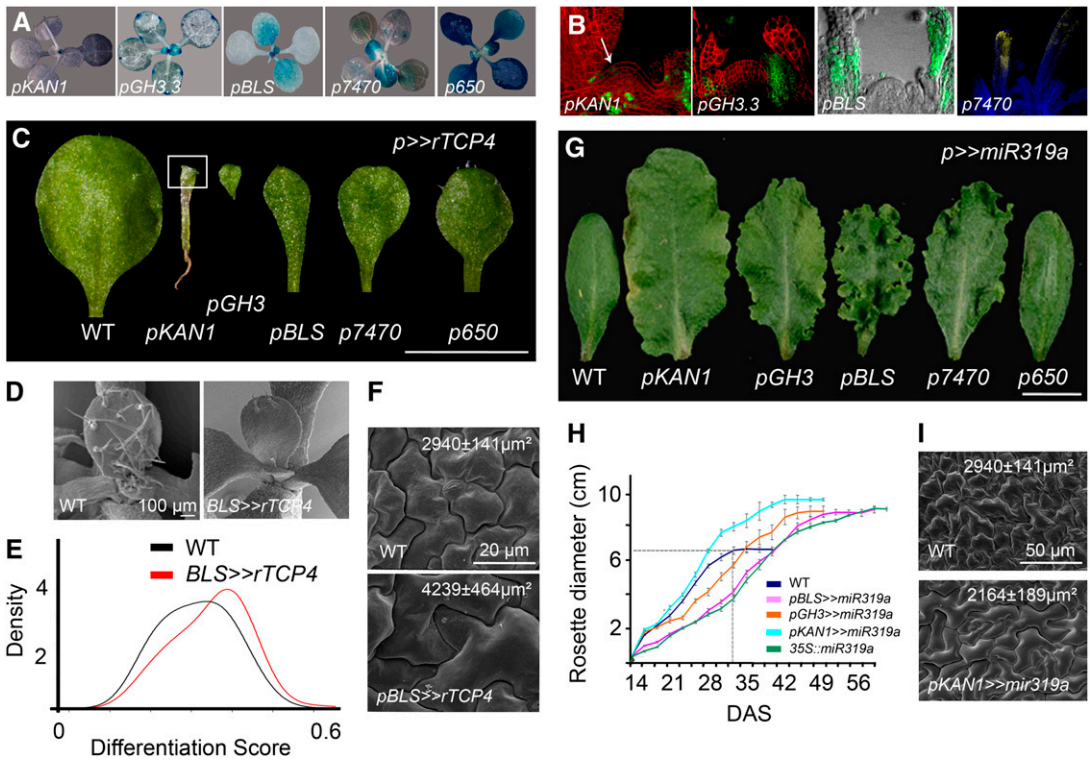

Figure 4. Temporal-Dependent Effects of Differentiation Regulators.

(A) GUS expression (blue color) mediated by selected promoters transiently expressed in developing leaves and allowing gene manipulation in sequential stages along leaf ontogeny.

(B) Confocal images of dissected 14-DAS shoot apices expressing OP:GFP (or OP:dsRed for *p7470*) transactivated by the promoters in **(A)**. GFP fluorescence is in green, dsRed fluorescence is in yellow, and red and blue are calcofluor white. Note the early and brief expression in *pKAN1* (P0 marked by an arrow) and the sequential initiation and caesurae of expression mediated by the other promoters. For *p650*, the onset of leaf expression could not be captured by a SAM-containing frame and thus was not included.

(C) Fully expanded first leaf of plants ectopically expressing miR319-insensitive *TCP4* (*rTCP4*) by the promoters shown in **(A)**. The earlier the expression initiates, the more severe the dwarfing effects are. Thus, *pKAN1>>rTCP4* plants are made of miniature cotyledons only (boxed).

(D) to **(F)** Comparisons of wild-type and *pBLS>>rTCP4* plants.

(D) A scanning electron microscopy image of 14-DAS shoots used for DDI and DMI analyses. Cotyledons and leaves 1 and 2 were removed.

(E) Distribution of differentiation scores is shifted in *pBLS>>rTCP4* plants.

(F) Adaxial epidermis of fully expanded sixth leaf of the plants in **(D)**. Average epidermal cell size is at the top left corner.

(G) Fully expanded 6th leaf of plants ectopically expressing *miR319a* by the promoters shown in **(A)**.

(H) Growth kinetics of the plants ectopically expressing *miR319a*. Note the similarity of *pBLS>>miR319a* and *35S:miR319a*. Rosette diameters were measured until a plateau was reached. Gray bars, SE; dotted line, growth cessation in the wild type.

(I) Adaxial epidermal cells of the wild type and *pKAN1>>miR319a* have comparable cell shape. Average epidermal cell size is at the top left corner. Bars = 1 cm in **(C)** and **(G)**; other bars are as labeled.

and *p650* is restricted to expanding lamina (Figures 4A and 4B) in a pattern that complements *CYCB1;2:GUS*. The array of these stage-specific selected promoters permitted analysis of transient expression in sequential time windows throughout the developing leaf ontogeny. These time windows are reminiscent of the patterns in Figure 1B and were used to dissect the consequences of precocious or delayed onset of the differentiation process. Manipulation of select *CIN-TCP* expression was performed either via *miR319a* overexpression or via ectopic expression of a miR319-resistant version of *TCP4* (*rTCP4*).

Early expression of *rTCP4* was previously reported to result in plants with two miniature fused cotyledons (Palatnik et al., 2003), similar to effects found with *pKAN1>>rTCP4* plants. A few miniature leaves were formed when *rTCP4* was driven by *pGH3.3* (Figure 4C), subsequently ending in shoot development arrest. As expected, ectopic expression of *rTCP4* within the PM phase, using later promoters such as *pBLS* and *p7470*, resulted in a milder effect, producing small leaves that, in the case of *pBLS*, were also narrower. Later activation of *rTCP4* using the *p650* promoter, which has the broadest activity domain, resulted in nearly normal leaves (Figure 4C).

Leaves of the mildly affected *pBLS>>rTCP4* plants were next subjected to more detailed morphological and DDI analyses. In young plants assayed at 14 DAS, the effects of ectopic *rTCP4*

were evident by the almost complete loss of trichomes (Figure 4D). In addition, the differentiation score distribution of *pBLS>>rTCP4* plants showed an overall shift relative to same age wild-type ones (Figure 4E, Table 1). Consistent with this, the epidermal cells of the mature *pBLS>>rTCP4* leaves were more than double the size of the wild type (Figure 4F), implying that these small leaves were made of far fewer cells, a likely reflection of a brief PM phase. The strong effects of precocious TCP4 expression, and more significantly, the mild effects stimulated by the strong and widespread late promoters, are consistent with a precise phase-dependent potential of *TCP4* in differentiation promotion and illustrate the significance of temporal regulation of such heterochronic factors for overall organ growth.

Delayed Activation of the Leaf Maturation Program Yields Larger Leaves

If progression of the organ maturation program is the primary role of the *CIN-TCPs*, then a transient delay in their onset would allow additional cell divisions to be followed by normal maturation and cell expansion, and, hence, larger leaves made of normal cells. Therefore, the stage-specific selected promoters were next used to supplement the endogenous expression of *miR319a* in wild-type leaves. Strikingly, plants expressing *miR319a* driven by *pKAN1* or *pGH3.3* promoters, which are expressed primarily during the primordia initiation stage, developed leaves that were 3 and 2.5 times, respectively, larger than the wild type (Figure 4G, only fully expanded 6th leaf is shown). By contrast, slightly later activation of *miR319a* by the *pBLS* promoter resulted in plants with slow-growing curled leaves, mimicking the effects of the ubiquitous *35S* promoter. Later activation of *miR319a* with promoters such as *p7470* or *p650* resulted in mild or no effects, respectively (cf. Figures 3E and 4G). That *pBLS>>miR319a* plants are most similar to *35S:miR319a* plants (Figure 4G and 4H) suggests either that *pBLS* drives the strongest expression or that its expression marks the time window when CIN-TCP activities are most required to promote lamina maturation. Indeed, GUS expression driven by the various promoters was most prominent in *p650* (Figure 4A), a promoter that stimulated no effects when used to transcativate miR319a. In agreement, the strongest downregulation of *TCP4* RNA was found in *pGH3* and *pBLS>>miR319a* plants (see Supplemental Figure 6B online), suggesting significant overlap in the promoter activities and TCP4 expression. That no further enhancement of the phenotypes was obtained upon selfing of any of the various transgenic lines further argues for the significance of timely versus quantitative regulation of the CIN-TCPs as a prime mode of leaf form regulation. Of striking appearance were *pKAN1>>miR319a* leaves that were much larger than the wild type (Figure 4G) yet displayed nearly normal levels of TCP4 (see Supplemental Figure 6B online). It is unlikely that the abaxial expression of the promoter accounts for these effects, as transactivation of *miR319a* by the *pFILAMENTOUS FLOWER* driver, which like *pKAN1* drives abaxial expression, but for an extended period, resulted in strongly curled lamina, as found with the *pBLS* driver.

Under the conditions used, growth of wild-type leaves was maintained for slightly >30 d, whereas growth of *pBLS>>miR319a* or *35S:miR319a* leaves lasted >50 d (Figure 4H). The relatively slow rate of leaf expansion that characterized this extended period is a reflection of the absence of the extensive cell expansion phase typical of the SM stage. By contrast, expansion rate was not altered in *pKAN1>>miR319a* plants (Figure 4H), leaf epidermal cells retained their normal jigsaw shapes, and epidermal cell size was nearly normal (Figure 4I). Overall, these results show that changes in the onset of endogenous maturation programs can have dramatic consequence on organ size, allowing it to bypass restrictions imposed by simple manipulations of the cell cycle machinery (Tsukaya, 2003).

DISCUSSION

The Maturation Schedule Hypothesis and the Ever-Changing Leaf Composition

In this study, we used incremental changes and ephemeral combinations of gene expression to characterize leaf ontogeny (Figure 1). These changes are primarily made up of simple transient expression patterns of gradual increase, decrease, or with a single expression peak, whereas more complex patterns with multiple peaks and troughs are rare. The continuous changes in gene expression during leaf differentiation reflect sequential and transient activation of multiple regulators. Given the fact these changes, as captured by the DDI, can be robustly used to predict sample age, we can hypothesize a mechanism in which organ differentiation progresses through an internal self-advancing sequential maturation program, where the rate and time of advancement is regulated by a cell autonomous developmental clock (Figure 5A). Modifying the rate of the clock can be used, among other things, to determine organ size. A clock advancing through numerous steps can bridge the gap between the long process of leaf development and its regulation by short signaling intervals, measurable on a biochemical scale.

The described developmental cascade is reminiscent of the maturation schedule framework hypothesized by Freeling (1992) to describe maize (*Zea mays*) leaf development. In this system, age-dependent responses to several perturbations, mostly consisting of KNOX misexpression, illustrate a continuous, gradual, and predictable change of developmental potentials of leaf primordia. Our analyses of the *Arabidopsis* dicot leaf are in agreement with this model and extend its use into much later stages in leaf development.

Continuous developmental progression of early leaf differentiation has been recorded in the past on the basis of anatomical and morphological changes (Poethig and Sussex, 1985b). However, the use of such markers precluded the simple distinction between perturbations in cell fate specification and in developmental progression (heterochronic) mechanisms, in which cell fate disruptions are secondary. The transcriptome-based DDI offers an assay to distinguish between the two. For example, the distribution of differentiation scores was retained in the cell fate mutant *gl1* that lacks trichomes, while reduction in the levels of heterochronic genes such as the *CIN-TCPs* stimulated a dramatic distribution shift toward less differentiated values (cf. Figure 2A with 3J or 4E). Orderly organized lineage maps have

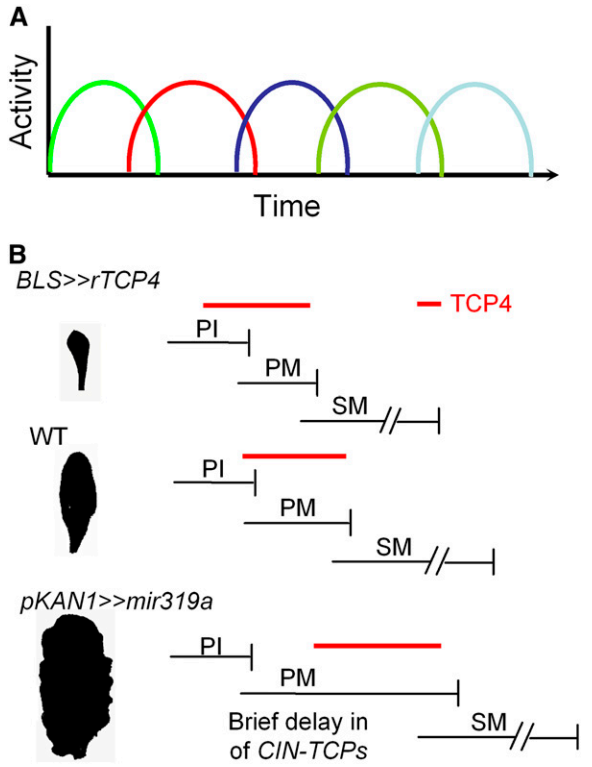

Figure 5. The Organ Differentiation Program and Its Responses to Perturbed Heterochronic Regulators.

(A) A model for a program of unidirectional progression along ontogeny through a successive expression of heterochronic regulators, represented by different colors. When such a maturation schedule is made of numerous steps, an ongoing regulation of differentiation is feasible.
(B) Temporal CIN-TCP activities (represented by the red line) and its impact on leaf form (shown at the left). In the wild type during primordium initiation (PI), most *CIN-TCPs* are transcriptionally repressed by *miR319*. Upon lamina initiation, sequential CIN-TCP activities promote the transition from PM into the cell expansion and SM phase. Precocious TCP4 expression as in *pBLS>>rTCP4* causes premature transition into the SM phase and small leaves. A mild delay in CIN-TCP activation as in *pKAN1>>miR319a* leaves prolongs the PM phase but permits normal entry into the SM phase, yielding much larger leaves.

facilitated the identification of many heterochronic regulators in worms (Slack and Ruvkun, 1997). The adoption of transcriptome dynamics–based analyses to characterize organ differentiation regulators can therefore have widespread use in many other organisms where lineage maps are not available. However, while a maturation schedule signature can be captured by DDI, its underlying molecular mechanism remains to be elucidated.

The Role of Class II TCPs in Organ Growth

Many class II TCP genes, the clade that includes the CIN-TCPs examined in this study, have been morphologically analyzed to date, and many were implicated in regulation of organ growth and differentiation (this study; Nath et al., 2003; Palatnik et al., 2003; Koyama et al., 2007; Ori et al., 2007). However, assigning them a general role in coordination of these processes has been complicated by their conflicting effects on different plant organs. For example, loss of *Antirrhinum CIN* results in excessive growth in leaves and limited growth in petals (Nath et al., 2003; Crawford et al., 2004). Furthermore, overexpression of another *Antirrhinum* class II TCP gene, *CYCLOIDEA* (*CYC*) in *Arabidopsis*, stimulated large petals made of large cells and small leaves made of small cells (Costa et al., 2005). Even in the same organ, conflicting growth effects were documented. Ectopic expression of the *Gerbera* (Asteraceae) *CYC* gene caused enlargement and fusion of petals of the symmetric disc flowers, but a reduction in the size of both leaves and the asymmetric ray flower petals (Broholm et al., 2008). One mechanism that has been suggested for class II TCP activity is a role in regulation of cell cycle genes (Nath et al., 2003; Li et al., 2005). Indeed, upregulation of *cyclin D3b*, accompanied by extended mitotic cell division, is observed in *Antirrhinum cyc* flowers and *cin* leaves (Gaudin et al., 2000; Nath et al., 2003). Furthermore, *CIN* is expressed predominantly in proliferating cells (Crawford et al., 2004). However, this association may not reflect direct regulation and cannot readily account for other TCP-stimulated phenotypes, such as organ fusion (Broholm et al., 2008). Furthermore, while *cin-tcp* leaves exhibit extended cell division in later stages of leaf development (Figure 3K), analysis of the same leaves at earlier stages revealed the opposite trend (i.e., downregulation of the mitotic cell division transcriptional signature) (Figure 3J).

How can these contrasting effects be reconciled? Our analysis revealed that knockout of five *CIN-TCP* genes during early *Arabidopsis* leaf development caused a dramatic and coordinated transcriptome change, involving hundreds of genes, and mimicking the transcriptome of leaves of younger age. We propose that, in the framework of the sequential maturation scheme, the TCPs are heterochronic genes acting at early stages of lamina development to regulate a developmental clock and that cell cycle machinery regulation by the TCPs is of indirect nature. Consistent with this view, the brief delay of TCP activity in *pKAN1>>miR319a* plants introduced a delay in the maturation program allowing the incorporation of more cells into the developing leaf in a manner that had little effect on later patterning programs (Figures 4G to 4I and 5B). Taken together, our data provide evidence for a primary role of *CIN-TCPs* in promotion of tissue maturation. That late inactivation of the *CIN-TCPs* has either minor or no effect on blade development (Figure 4G), although levels of the *miR319* target gene are reduced (see Supplemental Figure 6 online), implies that maturation regulation is mediated primarily by early *CIN-TCP* expression. Unfortunately, low expression levels precluded detailed spatial analyses of initial *CIN-TCP* expression in emerging leaf primordia. However, both *TCP3* and *TCP4* are initially expressed in the distal domain of the cotyledons (Palatnik et al., 2003; Koyama et al., 2007), the domain that will mature first, and excluded proximally. Similar exclusion was evident in tomato leaf and leaflet primordia expressing *LA*, which was mirrored by distal exclusion of *miR319* expression (Ori et al., 2007). In maturing leaves, however, gradual distal exclusion was observed for factors such as the *Antirrhinum CIN*, marking the cell cycle arrest front. This expression may correspond to cues set by the early *CIN-TCP* expression and may not be directly involved in the maturation process.

The analysis of root maturation (see Supplemental Figure 3 online) revealed that while the mitotic cell division machinery is shared among shoot and root, the maturation schedule itself is organ specific. Rates of cell proliferation and overall organ growth vary between the different stages of organ development; therefore, altering the relative duration of each stage can have a marked effect on the final organ form. The organ-specific maturation schedule therefore underlies differences in organ morphology and also accounts for unique responses to altered expression of class II TCPs.

METHODS

Plant Material

All plants except for T-DNA insertion lines and their controls (*35S:miR-3TCP*, Col), were of the L*er* background. Plants were grown under fluorescent light: long day for morphological analyses and short day for RNA collection (16 and 10 h light, respectively, 22°C). Age is expressed in DAS for 48 h at 4C°. T-DNA insertion alleles were as follows: *tcp17* (Salk_147288; Alonso and Stepanove, 2003), *tcp5* (SM_3_29639), and *tcp13* (SM_3_23151). In all cases, insertions were verified to lie within the gene's open reading frame. Primers used for verification of the insertion are listed in Supplemental Table 1 online. Multiple mutant plants were generated by conventional breeding. The mutant line *gl1-1* was previously described (Oppenheimer et al., 1991).

Plasmids and cDNA Clones

Driver and responder transactivation lines were generated and transformed into plants as described (Pekker et al., 2005). At least 15 different T1 plants were examined for each construct, and a selected representative with a single T-DNA insertion was used further. Primers used for cloned cDNA, pre-miRNAs, or promoters are described in Supplemental Table 1 online. For *pKAN1:LhG4* (Eshed et al., 2004), the gene's second intron was amplified by PCR and inserted 3′ of the promoter into a unique *Sal*I and *Bam*HI site of the original construct. The artificial *miR-3TCP* was designed for this study to target a conserved region within *TCP5*, *TCP13*, and *TCP17.* It was synthesized and subcloned as described (Alvarez et al., 2006). The *CYCB1;2:GUS* (Donnelly et al., 1999) construct line was a generous gift from John Celenza (Boston University).

Microscopy

Tissue preparation, histological analyses, tissue clearing, and GUS staining were performed as previously described (Pekker et al., 2005). Tissue preparation for detection of fluorescent signals and confocal microscopy was according to Goldshmidt et al. (2008). Scanning electron microscopy was performed using an XL30 ESEM FEG microscope (FEI) after standard tissue preparations (Alvarez et al., 2006).

Tissue Collection, RNA Preparation, and Microarray Hybridization

Plants were grown under short days to avoid floral transition, and tissue collection, using microscissors, of the different samples always took place at the same daily time interval (1 to 3 h after the beginning of the light period). In all experiments, two independent biological replicates were sampled. Total RNA (15 μg) was extracted with the RNeasy RNA isolation kit (Qiagen). Labeled cRNA was prepared and hybridized to Affymetrix ATH1 GeneChips according to the manufacturer's guidelines (Affymetrix).

RNA Gel Blot

Total RNA (~40 μg) was extracted from the aerial parts of 14-DAS short-day-grown plants using TRI reagent (Sigma-Aldrich) according to the manufacturer's instructions. Preparation of radiolabeled probe of *TCP4* coding region and RNA gel blot analysis were performed as by Alvarez et al. (2006).

Chip Analysis

Signal values were obtained using Affymetrix Microarray Suite software version 5.0. Expression values from each chip were normalized to its 50th percentile median and multiplied by a factor of 50. Genes with multiple or ambiguous probes were removed. Variation of data between replicates was evaluated, and as all replicates clustered together, further analysis was performed on mean values. Genes with normalized signal values of <30 in all samples were considered as absent and discarded from further analyses. This criterion resulted in 30.7% of the genes marked as absent. An arbitrarily twofold change criterion was selected to indicate that a marker gene was modified with age. Note that we do not claim a statistical significant change of individual genes, but rather for the whole cohorts of age-correlated genes. Normalization of gene values was performed by dividing each expression value by the maximum expression of this gene across all samples. Additional microarray raw data used in this work were downloaded from publicly available sources as detailed in Table 1 and processed and normalized as described above. To verify that the high prevalence of simple expression patterns detected among maturing leaves is not by chance, it was compared with patterns obtained from a randomly shuffled data set. In a permutated data set, gene expression values at each sample were randomly shuffled, maintaining the expression differences, but omitting possible order associated with age. Next, the prevalence of each expression pattern, gradient, and single or multiple peaks was determined. Following 100 reshufflings of the entire data set, the average number of genes in each pattern was computed. The significance of the observed patterns was determined with a χ^2 test ($P < 0.001$). Generation of 25 clusters using the K-means algorithm was performed in R (www.r-project.org). Clustering into 50 or 100 groups did not produce additional pattern types.

DDI and DMI Calculations

The DDI algorithm is based on samples of known developmental stages referred to as the Calibration Set. Identified age marker genes were selected from the calibration set, and differentiation scores scaled to age were extracted for each of these markers. Calibration set samples were ordered and each assigned an ordinal sequential numerical value with age increments of 1 (*x* axis in Figures 1E and 1F). Genes were considered as age markers if they were modified twofold with age and if at least one sample in the calibration set had an expression value (EV) > 30 and expression comprised of a single expression peak. That is, there exists only one *i*, which fulfills the conditions *EV(i)* > 30 AND *EV(i)* > *EV(i-1)* AND *EV(i)* > *EV(i+1)*, where *EV(i)* is the expression value of a gene in calibration sample number *i.*

Calculating differentiation scores for a given marker is based on different types of age predictions: (1) the expression value is equal to or higher than the peak expression value, yielding an age prediction equal to the peak; (2) two age predictions are produced, but the distance between them is <0.5 age increments, and in this case, the two age prediction are averaged; (3) two predictions are produced, but the distance is >0.5. To resolve this ambiguity, all markers fitting scenarios one and two are averaged to produce a crude age estimate. The prediction closer to the crude age estimate is preferred. If the expression value of an examined marker is called absent (<30) or is two times larger than the peak expression value, age prediction is discarded. Finally, all age predictions

are normalized to values ranging from 0 to 1 to produce differentiation scores. The DDI algorithm was executed in R (www.r-project.org). Scripts are available on request. Kernel density plots were produced using R, with a bandwidth of 0.1 for score distributions based on this study or AtGenExpress calibration sets and a bandwidth of 0.05 for calculations based on the combined calibration set where increased resolution was evident. Statistical significance analyses of DDI estimates were performed with JMP 6.0 (SAS).

To calculate the DMI, 73 previously characterized mitotic marker genes (Dewitte et al., 2007; genes used are listed in Supplemental Data Set 1 online) were analyzed. Gene expression values were normalized by dividing by the maximal value obtained among the four samples collected in this study (Apex-5DAS, Apex-14DAS, expanded leaves, and mature leaves). The average normalized expression of the remaining 73 was averaged to produce the DMI.

Accession Numbers

Microarray data have been deposited to the Gene Expression Omnibus database under series numbers GSE12691 and GSE12676.

Supplemental Data

The following materials are available in the online version of this article.

Supplemental Figure 1. Cluster Analysis of Gene Expression Patterns Modified with Age.

Supplemental Figure 2. Gene Expression Dynamics in Gradually Maturing L*er* Leaf Samples.

Supplemental Figure 3. Digital Maturation and Mitotic Indices of Leaves and Roots.

Supplemental Figure 4. Artificial miRNA that Simultaneously Targets the *TCP5-Like* Genes.

Supplemental Figure 5. Additional Phenotypes of Plants with Altered *CIN-TCP* Expression.

Supplemental Figure 6. Promoters Driving Sequential Expression of a Heterochronic Leaf Regulator.

Supplemental Table 1. Primers Used in the Course of This Study.

Supplemental Data Set 1. List of Marker Genes Used to Calculate DDI and DMI.

ACKNOWLEDGMENTS

The dedicated work of Carmit Sgula, Yael Tzurim, and Eviatar Shteiner is highly appreciated. We thank John Celenza and the ABRC Stock Center for providing plasmids and plant material and Markus Schmid, Jan Lohmann, and Detlef Weigel for generating the AtGenExpress developmental data. We thank Robert Fluhr, Naomi Ori, Eliezer Lifschitz, and members of our lab for comments and discussions and John Alvarez for help with the artificial miRNA design. The electron microscopy studies were conducted at the Irving and Cherna Moskowitz Center for Nano and Bio-Nano Imaging at the Weizmann Institute of Science. This work was funded by Research Grant 222-2 from the U.S.–Israel Binational Science Foundation, 863-06 from the Israel Science Foundation, 3767-05 from the U.S.–Israel Binational Agricultural Research and Development Fund, 824-05 from the German-Israeli Foundation for Scientific Research and Development, and from MINERVA. Y.E. is an Incumbent of the Judith and Martin Freedman Career Development Chair.

Received December 14, 2007; revised September 2, 2008; accepted September 9, 2008; published September 19, 2008.

REFERENCES

Alonso, J.M., and Stepanove, A.N. (2003). T-DNA mutagenesis in Arabidopsis. Methods Mol. Biol. **236:** 177–188.

Alvarez, J.P., Pekker, I., Goldshmidt, A., Blum, E., Amsellem, Z., and Eshed, Y. (2006). Endogenous and synthetic microRNAs stimulate simultaneous, efficient, and localized regulation of multiple targets in diverse species. Plant Cell **18:** 1134–1151.

Avery, G.S. (1933). Structure and development of the tobacco leaf. Am. J. Bot. **20:** 565–592.

Birnbaum, K., Shasha, D.E., Wang, J.Y., Jung, J.W., Lambert, G.M., Galbraith, D.W., and Benfey, P.N. (2003). A gene expression map of the Arabidopsis root. Science **302:** 1956–1960.

Brady, S.M., Orlando, D.A., Lee, J.Y., Wang, J.Y., Koch, J., Dinneny, J.R., Mace, D., Ohler, U., and Benfey, P.N. (2007). A high-resolution root spatiotemporal map reveals dominant expression patterns. Science **318:** 801–806.

Broholm, S.K., Tähtiharju, S., Laitinen, R.A., Albert, V.A., Teeri, T.H., and Elomaa, P. (2008). A TCP domain transcription factor controls flower type specification along the radial axis of the Gerbera (Asteraceae) inflorescence. Proc. Natl. Acad. Sci. USA **105:** 9117–9122.

Conlon, I., and Raff, M. (1999). Size control in animal development. Cell **96:** 235–244.

Costa, M.R., Fox, S., Hanna, A.I., Baxter, C., and Coen, E. (2005). Evolution of regulatory interactions controlling floral asymmetry. Development **132:** 5093–5101.

Crawford, B.C.W., Nath, U., Carpenter, R., and Coen, E.S. (2004). CINCINNATA controls both cell differentiation and growth in petal lobes and leaves of *Antirrhinum.* Plant Physiol. **135:** 244–253.

Day, S.J., and Lawrence, P.A. (2000). Measuring dimensions: The regulation of size and shape. Development **127:** 2977–2987.

Dewitte, W., Riou-Khamlichi, C., Scofield, S., Healy, J.M.S., Jacqmard, A., Kilby, N.J., and Murray, J.A. (2003). Altered cell cycle distribution, hyperplasia, and inhibited differentiation in Arabidopsis caused by the D-type cyclin CYCD3. Plant Cell **15:** 79–92.

Dewitte, W., Scofield, S., Alcasabas, A.A., Maughan, S.C., Menges, M., Braun, N., Collins, C., Nieuwland, J., Prinsen, E., Sundaresan, V., and Murray, J.A. (2007). Arabidopsis CYCD3 D-type cyclin link cell proliferation and endocycles and are rate-limiting for cytokinin responses. Proc. Natl. Acad. Sci. USA **104:** 14537–14542.

Donnelly, P.M., Bonetta, D., Tsukaya, H., Dengler, R.E., and Dengler, N.G. (1999). Cell cycling and cell enlargement in developing leaves of Arabidopsis. Dev. Biol. **215:** 407–419.

Eshed, Y., Izhaki, A., Baum, S.F., Floyd, S.K., and Bowman, J.L. (2004). Asymmetric leaf development and blade expansion in Arabidopsis are mediated by KANADI and YABBY activities. Development **131:** 2997–3006.

Freeling, M. (1992). A conceptual framework for maize leaf development. Dev. Biol. **153:** 44–58.

Fu, Y., Li, H., and Yang, Z. (2002). The ROP2 GTPase controls the formation of cortical fine F-actin and the early phase of directional cell expansion during Arabidopsis organogenesis. Plant Cell **14:** 777–794.

Gaudin, V., Lunness, P.A., Fobert, P.R., Towers, M., Riou-Khamlichi, C., Murray, J.A., Coen, E., and Doonan, J.H. (2000). The expression of D-cyclin genes defines distinct developmental zones in snapdragon apical meristems and is locally regulated by the Cycloidea gene. Plant Physiol. **122:** 1137–1148.

Goda, H., et al. (2008). The AtGenExpress hormone- and chemical-treatment data set: Experimental design, data evaluation, model data analysis, and data access. Plant J. **55:** 526-542.

Goldshmidt, A., Alvarez, J.P., Bowman, J.L., and Eshed, Y. (2008). Signals derived from YABBY gene activities in organ primordia

regulate growth and partitioning of Arabidopsis shoot apical meristems. Plant Cell **20:** 1217–1230.

Hagemann, W., and Gleissberg, S. (1996). Organogenetic capacity of leaves: The significance of marginal blastozones in angiosperms. Plant Syst. Evol. **199:** 121–152.

Kosugi, S., and Ohashi, Y. (2002). DNA binding and dimerization specificity and potential targets for the TCP protein family. Plant J. **30:** 337–348.

Koyama, T., Furutani, M., Tasaka, M., and Ohme-Takagi, M. (2007). TCP transcription factors control the morphology of shoot lateral organs via negative regulation of the expression of boundary-specific genes in Arabidopsis. Plant Cell **19:** 473–484.

Li, C., Potuschak, T., Colon-Carmona, A., Gutierrez, R.A., and Doerner, P. (2005). Arabidopsis TCP20 links regulation of growth and cell division control pathways. Proc. Natl. Acad. Sci. USA **102:** 12978–12983.

Lifschitz, E., Eviatar, T., Rozman, A., Shalit, A., Goldshmidt, A., Amsellem, Z., Alvarez, J.P., and Eshed, Y. (2006). The tomato FT ortholog triggers systemic signals that regulate growth and flowering and substitute for diverse environmental stimuli. Proc. Natl. Acad. Sci. USA **103:** 6398–6403.

Lyndon, R.F. (1998). The Shoot Apical Meristem: Its Growth and Development. (Cambridge, UK: Cambridge University Press).

Menges, M., de Jager, S.M., Gruissem, W., and Murray, J.A. (2005). Global analysis of the core cell cycle regulators of Arabidopsis identifies novel genes, reveals multiple and highly specific profiles of expression and provides a coherent model for plant cell cycle control. Plant J. **41:** 546–566.

Nath, U., Crawford, B.C., Carpenter, R., and Coen, E. (2003). Genetic control of surface curvature. Science **299:** 1404–1407.

Oppenheimer, D.G., Herman, P.L., Sivakumaran, S., Esch, J., and Marks, M.D. (1991). A myb gene required for leaf trichome differentiation in Arabidopsis is expressed in stipules. Cell **67:** 483–493.

Ori, N., et al. (2007). Regulation of LANCEOLATE by miR319 is required for compound-leaf development in tomato. Nat. Genet. **39:** 787–791.

Palatnik, J.F., Allen, E., Wu, X., Schommer, C., Schwab, R., Carrington, J.C., and Weigel, D. (2003). Control of leaf morphogenesis by microRNAs. Nature **425:** 257–263.

Pekker, I., Alvarez, J.P., and Eshed, Y. (2005). Auxin response factors mediate Arabidopsis organ asymmetry via modulation of KANADI activity. Plant Cell **17:** 2899–2910.

Poethig, R.S. (1997). Leaf morphogenesis in flowering plants. Plant Cell **9:** 1077–1087.

Poethig, R.S. (2003). Phase change and the regulation of developmental timing in plants. Science **301:** 334–336.

Poethig, R.S., and Sussex, I.M. (1985a). The cellular parameters of leaf development in tobacco: A clonal analysis. Planta **165:** 170–184.

Poethig, R.S., and Sussex, I.M. (1985b). The developmental morphology and growth dynamics of the tobacco leaf. Planta **165:** 158–169.

Reinhardt, D., Frenz, M., Mandel, T., and Kuhlemeier, C. (2005). Microsurgical and laser ablation analysis of leaf positioning and dorsoventral patterning in tomato. Development **132:** 15–26.

Schmid, M., Davison, T.S., Henz, S.R., Pape, U.J., Demar, M., Vingron, M., Scholkopf, B., Weigel, D., and Lohmann, J.U. (2005). A gene expression map of *Arabidopsis thaliana* development. Nat. Genet. **37:** 501–506.

Schwab, R., Palatnik, J.F., Riester, M., Schommer, C., Schmid, M., and Weigel, D. (2005). Specific effects of microRNAs on the plant transcriptome. Dev. Cell **8:** 517–527.

Slack, F., and Ruvkun, G. (1997). Temporal pattern formation by heterochronic genes. Annu. Rev. Genet. **31:** 611–634.

Tsukaya, H. (2003). Organ shape and size: A lesson from studies of leaf morphogenesis. Curr. Opin. Plant Biol. **61:** 57–62.